

# PCCP

Accepted Manuscript



This is an *Accepted Manuscript*, which has been through the Royal Society of Chemistry peer review process and has been accepted for publication.

*Accepted Manuscripts* are published online shortly after acceptance, before technical editing, formatting and proof reading. Using this free service, authors can make their results available to the community, in citable form, before we publish the edited article. We will replace this *Accepted Manuscript* with the edited and formatted *Advance Article* as soon as it is available.

You can find more information about *Accepted Manuscripts* in the [Information for Authors](#).

Please note that technical editing may introduce minor changes to the text and/or graphics, which may alter content. The journal's standard [Terms & Conditions](#) and the [Ethical guidelines](#) still apply. In no event shall the Royal Society of Chemistry be held responsible for any errors or omissions in this *Accepted Manuscript* or any consequences arising from the use of any information it contains.

# Strong electric fields at a prototypical oxide/water interface probed by *ab initio* molecular dynamics: MgO(001)

Sara Laporte,<sup>\*a</sup> Fabio Finocchi,<sup>b</sup> Lorenzo Paulatto,<sup>a</sup> Marc Blanchard,<sup>a</sup> Etienne Balan,<sup>a</sup> François Guyot<sup>a</sup> and Antonino Marco Saitta<sup>a</sup>

Received Xth XXXXXXXXXXXX 20XX, Accepted Xth XXXXXXXXXXXX 20XX

First published on the web Xth XXXXXXXXXXXX 200X

DOI: 10.1039/b000000x

We report a density-functional theory (DFT)-based study of the interface of bulk water with a prototypical oxide surface, MgO(001), and focus our study on the often-overlooked surface electric field. In particular, we observe that the bare MgO(001) surface, although charge-neutral and defectless, has an intense electric field on the Å scale. The MgO(001) surface covered with 1 water monolayer (1ML) is investigated via a supercell accounting for the experimentally-observed (2 × 3) reconstruction, stable at ambient temperature, and in which two out of six water molecules are dissociated. This 1ML-hydrated surface is also found to have a high, albeit short-ranged, normal component of the field. Finally, the oxide/water interface is studied via room-temperature *ab initio* Molecular Dynamics (AIMD) using 34 H<sub>2</sub>O molecules between two MgO(001) surfaces. To our best knowledge this is the first AIMD study of the MgO(001)/liquid water interface in which all atoms are treated using DFT and including several layers above the first adsorbed layer. We observe that the surface electric field, averaged over the AIMD trajectories, is still very strong on the fully-wet surface, peaking at about 3 V/Å. Even in the presence of bulk-like water, the structure of the first layer in contact with the surface remains similar to the (2 × 3)-reconstructed ice ad-layer on MgO(001). Moreover, we observe proton exchange within the first layer, and between the first and second layers – indeed, the O-O distances close to the surface are found to be distributed towards shorter distances, a property which has been shown to directly promote proton transfer.

## 1 Introduction

The impressive amount of works dedicated to the interfaces between water and oxide surfaces is motivated by their relevance to many different areas<sup>1</sup>: environmental sciences, electrochemistry<sup>2,3</sup>, catalysis and biochemistry<sup>4</sup>. Among the complexity that emerges, the issue of the influence of the surface on the properties of water is a leitmotiv in most studies. For instance, the atomic structure of the crystal surface plays a crucial role in determining proton transfer<sup>5</sup>, in forming silanol groups and small rings at bioactive surfaces<sup>6</sup> or strengthening silanol bonding at crystalline silica surfaces<sup>7</sup>, in influencing water diffusion at hydrated layered solids<sup>8</sup>, in promoting anisotropic bonding and confinement to SiC(100)<sup>9</sup>, and in allowing the coexistence of hydrophilic and hydrophobic interactions between talc surfaces and water<sup>10</sup>. From previous works, it appears that one or more water layers at the interface have different static and dynamical properties from bulk water, although the thickness of such a region depends

crucially on the surface structure and charge, and on the presence of dissolved ions. Also exciting is the perspective to tune the properties of interfacial water by changing the oxide support. Such complexity calls for settled models of prototypical water/oxide interfaces. Although less relevant in geochemistry, biology and catalysis than other oxide surfaces, the (001) surface of MgO shows a simple atomic and electronic structure that is well established in dry conditions. Less clear is the interaction between magnesium oxide and water. The shape of MgO crystallites changes from cubic to octahedral when they are exposed to water<sup>11</sup>. The dissolution process of MgO(001) is rather fast in acidic solutions and deeply modifies the surface morphology<sup>12</sup>, in a process dominated by kinetics. In contrast, at low water coverage (up to a monolayer) and for time lapses of order of a few hours, water adsorption on MgO(001) is dominated by thermodynamics. The isolated H<sub>2</sub>O molecule spontaneously dissociates on low-coordinated surface sites, such as steps and kinks, but not on the flat (001) terrace<sup>13</sup>, at odds with other alkali-earth oxides like CaO and BaO. However, hydrogen-bonded water ad-molecules on MgO(001) can dissociate, giving rise to characteristic hydroxyl groups consisting of a surface O and a proton coming from the ad-molecule<sup>14</sup>. This theoretical picture is corroborated by several experimental observations of the progressive onset of water dissociation as a function of

<sup>a</sup> Sorbonne Universités, Université Pierre et Marie Curie Paris 06, CNRS, Muséum National d'Histoire Naturelle, IRD, UMR 7590, Institut de Minéralogie, de Physique des Matériaux et de Cosmochimie, E-mail: sara.laporte@impmc.upmc.fr

<sup>b</sup> Sorbonne Universités, Université Pierre et Marie Curie Paris 06, CNRS, UMR 7588, Institut des NanoSciences de Paris

the increasing water coverage<sup>15,16</sup>. In the limit of a complete water monolayer on MgO(001), several ordered reconstructions were observed as a function of temperature<sup>17</sup>. All of them feature a variable proportion of hydroxyl groups resulting from the dissociation of some water ad-molecules, a picture that was originally proposed for the  $(2 \times 3)$ -reconstructed water monolayer on MgO(001) on the basis of first-principles simulations<sup>18</sup>. The use of Density Functional Theory reconciled theory with experiments, as empirical force fields, most of which do not allow for water dissociation, were not able to provide an explanation for these reconstructions<sup>19</sup>.

For water coverage above one monolayer, the experimental observations are rather scarce. Although many studies indicated that water organizes into very ordered layers close to the surface, a precise knowledge of the extent and the detailed characteristics of such organization as a function of the surface morphology is still fragmentary. Polycrystalline CaO was found to be much more reactive than MgO towards water<sup>20</sup>. The enthalpy of adsorption of water on MgO varied significantly from 1/2 to 3 monolayers, which was attributed to a stronger interaction between the first layer and the surface than between the next water ad-layers<sup>21</sup>. Experimental data at water pressure close to the ambient are also biased by a possible carbon contamination and by the fact that a steady state of the system might not be completely reached<sup>16</sup>. On the theoretical side, several simulations considered higher water coverage than one monolayer, but most of them used empirical models. By using a shell-model potential for water, the adsorption of the first water monolayer onto MgO(001) was shown to disrupt ordering in the next layers, leading to decreasing water density close to the surface<sup>22</sup>. This puzzling result was contradicted by an integral equation based 3D-RISM theory<sup>23</sup>, which yielded a water distribution along  $z$  in disagreement with that obtained in ref.<sup>22</sup>. The structural and dynamical properties of hydrated MgO nanoparticles were investigated through molecular dynamics using empirical interatomic potentials<sup>24</sup>. While highly ordered water layers appeared at the interface with the flat (001) surface, water coordination number, residence times and other properties were affected by the presence of corners and edges on surfaces with higher Miller indices. A significant ordering of water molecules, which are almost parallel to the surface in the two layers close to MgO(001), was found through molecular dynamics using a Born-Mayer-Buckingham interatomic potential for MgO and a flexible model for water<sup>25</sup>. Translational and orientational order parameters recovered their values for bulk water at about 3-4 layers from the surface. These features correlated with changes in the vibrational density of states of water. All the previous simulations were based on classical force fields and did not take into account water dissociation nor the influence it could have on the structure and the dynamical properties of the next water layers. An exception was provided by a first-

principles study of the interface between ice and MgO(001)<sup>26</sup>. However, the authors considered only four H<sub>2</sub>O layers on top of a  $\sqrt{2} \times \sqrt{2}$  surface unit cell and conducted structural optimization at 0 K. The system dimension and the absence of dynamics hindered the comparison with experimental data as well as any discussion of the extent of water ordering. Very recently, it was shown that defective MgO(001) surfaces, involving hydrated Mg<sup>2+</sup> ions above the surface and cation vacancies filled with protons, are more stable than a flat, hydrated MgO(001) surface<sup>27</sup>. As far as the surface electric field is concerned, Kelvin probe microscopy can be used to determine the surface work function with a lateral resolution of the order of few nm<sup>28</sup>. Other local probes of the surface electric field are ad-molecules themselves, such as carbon monoxide. The shift of its vibrational frequency with respect to the gas phase is connected to the local charge and electric field of the cation sites on the surface<sup>29</sup>. However, these probes cannot easily be used at the water/oxide interface. Furthermore, there are very few studies that have attempted to calculate the electrostatic properties of a water/oxide interface in order to make the link between coarse-grained Electric Double Layer (EDL) theories and the reality of the local electric field. This is largely due to problems arising from interacting periodic replicas, which can be overcome when there is vacuum in the supercell<sup>30</sup>, but become harder to work with when the supercell is 'filled' with water. For this reason studies reporting values of the electric field at an oxide interface require the surface to be neutral to minimise interactions between periodic replicas. Vlcek *et al.*<sup>31</sup> reported fields of about 6 V/Å at the SnO<sub>2</sub>/water interface using static *ab-initio* calculations. D'Ercole *et al.*<sup>32</sup> provide electrostatic potential maps of defects at MgO and CaO surfaces, and the resulting field values are of several V/Å extending 2 Å to 3 Å from the position of the surface atom. Here, we study the influence of the MgO(001) surface on the water density profile and the extent of molecular dissociation from the surface layer into the bulk of the liquid. We use *ab initio* molecular dynamics (AIMD), which can account for a correct description of both bonding and electric fields<sup>33</sup>, and the main statistical properties of liquid water at  $T \approx 300$  K. In particular, we focus on the behaviour of the surface electric field, how it is screened by the water molecules and, reciprocally, its influence on the structure of water.

## 2 Computational Details

The interfaces investigated were studied using *ab initio* molecular dynamics in which the interatomic forces are calculated in the density functional theory (DFT) framework. We used the PW (plane waves) code of the QUANTUM ESPRESSO<sup>34</sup> package, with ultrasoft pseudo potentials and the PBE functional which includes generalized gradient corrections. The cut-off for the plane-waves expansion was fixed at 35 Ry, and

for the charge density 280 Ry, after convergence tests. The London dispersion correction<sup>35</sup> was used to take into account Van der Waals forces, which are known to be important in the structuring of liquid water. Due to the use of supercells only the  $\Gamma$  point was taken into account in the Brillouin zone. We used the optimal theoretical lattice parameter for MgO  $a = 4.22$  Å. The MgO(001) slab is 12.66 Å thick with 7 MgO layers in the  $z$  direction, with the central layer clamped at bulk atomic positions, followed by 19.83 Å of vacuum or water. This distance between the periodic replicas of the slab was chosen by checking energy convergence so as to avoid interaction between replicas, and optimised with respect to total energy when 34 water molecules were added. The average density of water between the slabs has been determined from test calculations, in which several water configurations were constructed at varying distance between the two slab surfaces. By energy minimisation, we found the most stable configuration at 0.98 g/cm<sup>3</sup>, in good agreement with the experimental density of water. The  $x$  and  $y$  dimensions of the supercell were chosen to match the  $(2 \times 3)$  reconstruction of the known water ad-layer on MgO(001). The dimensions of the supercell are thus  $(\frac{2}{\sqrt{2}} \times \frac{3}{\sqrt{2}} \times 7.7)a$  or  $(5.97 \times 8.95 \times 32.49)$ Å. For simplicity, the two surfaces of the slab in contact with water are represented at  $\pm z_s$  with  $z_s = 10.10$  Å. For molecular dynamics the Born-Oppenheimer approximation was used, meaning that electronic degrees of freedom are fully relaxed in between each AIMD timestep. The timestep used was 0.38 fs. The Verlet algorithm was used to integrate the equations of motion and temperature rescaling was used to keep the average simulation temperature at 300 K with a tolerance of  $\pm 50$  K.

### 3 Results

#### 3.1 Electric field at the bare MgO surface

The electric field at a given position  $\mathbf{r}$  can be obtained in *ab initio* calculations from the electrostatic potential, which is the sum of the ionic and Hartree potentials  $V_I$  and  $V_H$

$$V_{\text{E.S.}}(\mathbf{r}) = V_I(\mathbf{r}) + V_H(\mathbf{r}) \quad (1)$$

$$\mathbf{E}(\mathbf{r}) = -\nabla V(\mathbf{r}) \quad (2)$$

In our case the ionic potentials  $V_I$  are in fact ultrasoft pseudopotentials which include the effect of core electrons, and the Hartree potential is calculated for the valence electrons. Although pseudopotentials do not reproduce the right charge locally within the pseudization region (about 0.5 Å around the nuclei), these types of calculations reproduce the correct mean field in the areas between the ions, as verified by electron tomography measurements<sup>33</sup>. The electric field is a three-

dimensional vector field, which can be split into its components:

$$\mathbf{E}(\mathbf{r}) = E_x(x, y, z)\hat{\mathbf{e}}_x + E_y(x, y, z)\hat{\mathbf{e}}_y + E_z(x, y, z)\hat{\mathbf{e}}_z \quad (3)$$

where  $\hat{\mathbf{e}}_x$ ,  $\hat{\mathbf{e}}_y$  and  $\hat{\mathbf{e}}_z$  are the unit vectors along  $x$ ,  $y$  and  $z$ . For clarity and due to the symmetry of the system, we have chosen to look at the component of the field which is parallel to the surface normal  $E_z(x, y, z)$ . As this is a scalar field in three dimensions, we can either visualise it in a plane parallel to the surface for a given  $z_0$ :

$$E_z(x, y, z_0) \quad (4)$$

or as an average along  $x$  and  $y$ :

$$\bar{E}_z(z) = \frac{1}{A} \int dx \int dy E_z(x, y, z) \quad (5)$$

where  $A$  is the surface area of the supercell in the [001] direction. For  $\bar{E}_z(z)$  a macroscopic average filter has been applied to eliminate oscillations in the bulk and isolate interface contributions. This filter is a one-dimensional convolution:

$$\bar{\bar{E}}_z(z) = \frac{1}{b} \int_{z-b}^{z+\frac{b}{2}} \bar{E}_z(z') dz' \quad (6)$$

where the filter window  $b$  was chosen as the interlayer distance in MgO ( $b = a/2 = 2.11$ Å), unless specified otherwise. This coarse-graining is essentially analogous to that originally used for interfaces and sublattices<sup>36</sup> and has been shown to recover electrostatics at the atomic scale unbiased by the very short ranged oscillations<sup>33</sup>.

Figure 1 shows the electrostatic potential and electric field profiles at the MgO(001)/vacuum interface. For clarity the potential is shown as felt by the electrons – negative in the slab and positive in the vacuum. From analysis of the electrostatic potential we can calculate the work function, by comparing the vacuum level of the potential with the Fermi level. In this case the work function was calculated to be 5.19 eV, which is within 5% of the reported experimental value for the work function of the MgO(001) surface, 4.94 eV<sup>37</sup>, thus validating our value of the field and coarse-graining method. The broken symmetry in the surface normal direction results in a local asymmetry in the charge distribution at the interface – the electrons spill out into the vacuum and consequently there is an excess of positive charge just under the surface. This results in a strong surface dipole which is specific to each surface and contributes to the variation of the work function, and also results in an electric field<sup>33</sup>. As shown in figure 1, the electric field at the MgO(001)/vacuum interface is intense and permeates beyond the surface layer, although it is highly localised. There is a window extending to about 3 Å from the surface atoms in which the field is high enough to influence

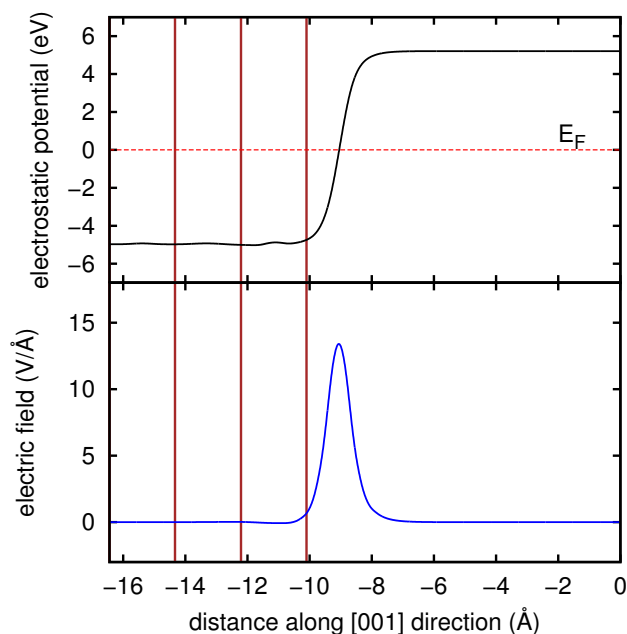


**Fig. 1** The average  $z$  electrostatic potential as felt by the electrons, and the electric field profile at the surface of a bare MgO(001) surface. The MgO planes are represented by vertical lines, and the Fermi level is shown. The work function can be calculated as the difference between the potential in the vacuum and the Fermi level.

potential adsorbates, their structure and reactivity. Although this view differs from the classical view of the electric field on top of an ionic solid, this approach is consistent with both average electrostatic properties of the surface (such as the work function described above) and with local electrostatics at the Angstrom scale. Figure 2 shows non-averaged profiles of the  $z$  component of the field directly on top of the surface  $\text{Mg}^{2+}$  and  $\text{O}^{2-}$  ions. Only points beyond the pseudo-potential cutoff radii are included. The behaviour is as expected, negative field on top of O and positive field on top of Mg. However there is overall a clear imbalance towards the positive  $z$ -direction due to the surface dipole, which is reflected in the positive value of the sum. Figure 3 shows the  $z$  component  $E_z(x, y, z_0)$ , with  $z_0$  at a height of  $2 \text{ \AA}$  from the surface, which corresponds to the adsorption height for water. The plot again shows the influence of the surface ions, with nevertheless a field imbalance towards the positive  $z$  axis.

### 3.2 Electric field with one monolayer of $\text{H}_2\text{O}$

A monolayer of water (1ML) on MgO(001) is known to exist in several configurations depending on temperature and pressure<sup>17</sup>. For this study we chose to use the  $(2 \times 3)$  reconstruction, which corresponds to the ‘high temperature’ configura-

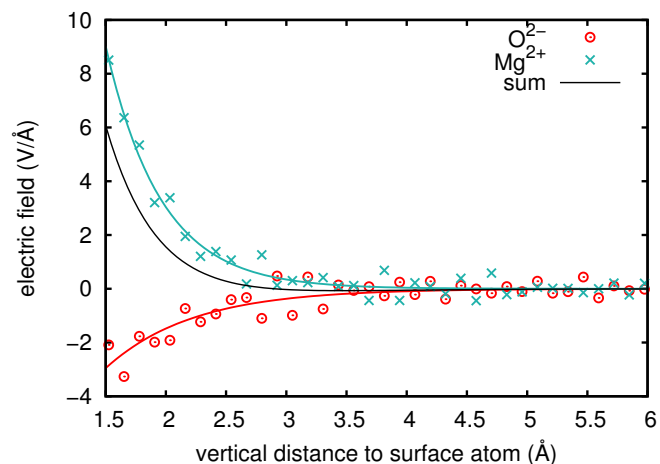


**Fig. 2**  $z$ -component of the electric field along the [001] direction, directly on top of each type of surface ion. The lines are exponential fits to the data.

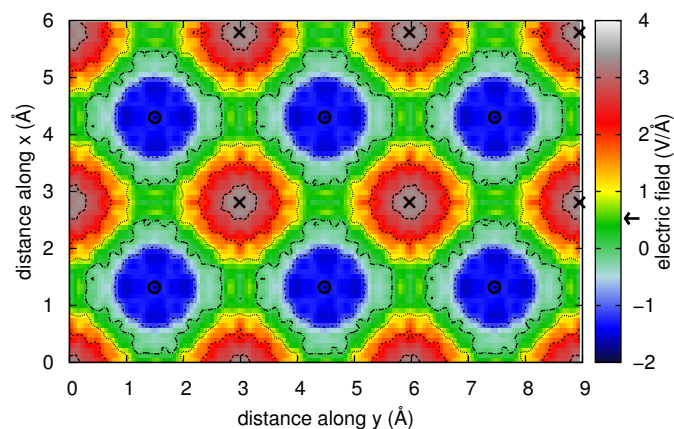


**Fig. 3**  $z$ -component of the electric field in an  $xy$  plane at  $2.0 \text{ \AA}$  from the surface layer of MgO(001). Lines are  $1.0 \text{ V/\AA}$  apart. Underlying atomic positions are labeled with crosses for Mg and circles for O. The arrow on the colourbar indicates the average value of the  $z$ -component of the field in this plane.

tion (stable between 185 K and 235 K in UHV conditions<sup>17</sup>). In this reconstruction two out of six water molecules are dissociated as shown in figure 4. Initially the six water molecules were placed on top of MgO(001) and the positions allowed to relax. This resulted in spontaneous dissociation of two water molecules, with no energy barrier, in a configuration which was slightly different from the one in figure 4, but which exhibits the same number of OH groups on the surface and has the same symmetry ( $2 \times 3$  with a glide-plane). We still chose however to use the configuration in figure 4 because it is accepted as the most stable configuration in the literature and because its energy was lowest. It is likely that several metastable analogues of this configuration exist, especially at non-zero temperatures, but due to the small size of the simulation box we chose for the following to remain with the most stable configuration at 0 K, even later on when several layers of water were added. Figure 5 shows the electric field profile in the 1ML case. A first peak occurs within the adsorbed layer at the height of the adsorbed  $H^+$  ions, and the second peak seems analogous to that in the bare surface case, *i.e.* intense, highly localised, but permeating a few Ångströms beyond the surface. This peak is not as intense as in the bare surface case, which is a sign of screening by the  $H_2O$  molecules. Figure 6 shows the profile in the  $xy$  plane at a height of 4 Å from the surface, so about 2 Å from the adsorbed monolayer. At this height the underlying surface structure is not longer ‘visible’ in the field profile, and is instead screened by the less ordered adsorbed monolayer. We notice zones of positive and negative  $z$  fields corresponding to local water dipoles, as well as small scale oscillations which would probably become irrelevant when taking into account the dynamics of the system. Such complexity calls for a coarse-grained description of the electric field, especially when we consider its effect on the structural and dynamical properties of the water above the first ad-layer. For the case of the water/MgO interface with more than a water ad-layer, we will thus retain the profile along  $z$ :  $\bar{E}_z(z)$ .

### 3.3 The MgO/water interface: structure and electric field

Starting from the ( $2 \times 3$ ) monolayer reconstruction, 22 water molecules were added to the simulation cell to ‘fill up’ the vacuum between the slabs, resulting in a simulation consisting of 7 MgO layers in the [001] direction followed by 34 water molecules, 4 of which are dissociated on the surface (2 on each side). Before starting the simulation, the 22 water molecules were placed randomly in a box without MgO and AIMD was performed at 300 K for a few picoseconds. From this simulation, the initial positions were placed in between the MgO slabs, and the AIMD simulation was started with several subsequent rescaling steps of increasing temperature. Eventually the target temperature of 300 K was reached,

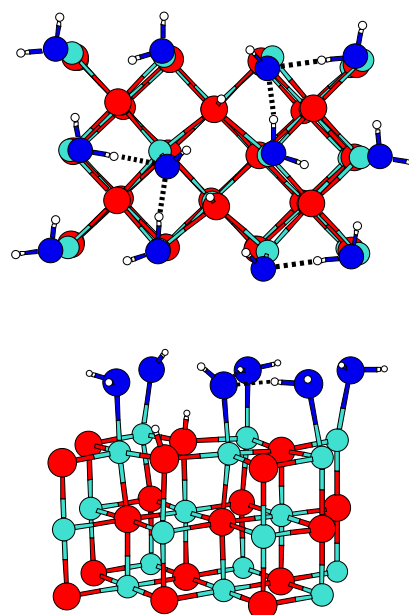


**Fig. 4** Top view and side views of the unit surface of the ( $2 \times 3$ ) reconstruction of water on MgO. The Mg atoms are turquoise and the oxygen atoms belonging to the slab are red, while the oxygen atoms of the water monolayer are shown in blue.

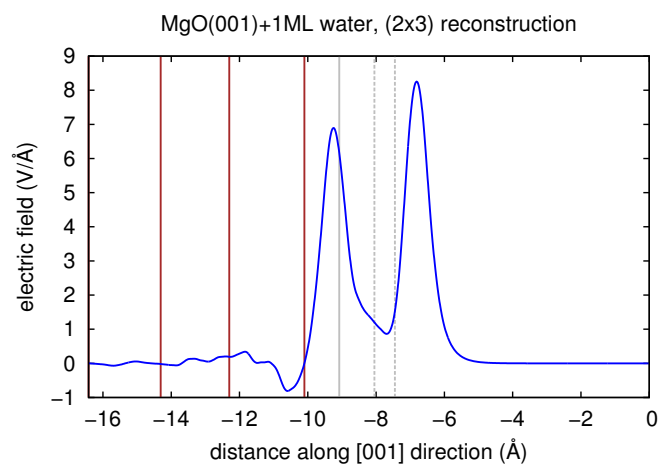


**Fig. 5** Electric field profile of MgO(001) with a monolayer of water adsorbed, in a ( $2 \times 3$ ) reconstruction with partial dissociation. The vertical lines represent the MgO planes (brown), the average position of the adsorbed  $H^+$  ions (solid grey) and the upper and lower bounds of the positions of the adsorbed water molecules and  $OH^-$  ions (dotted grey)

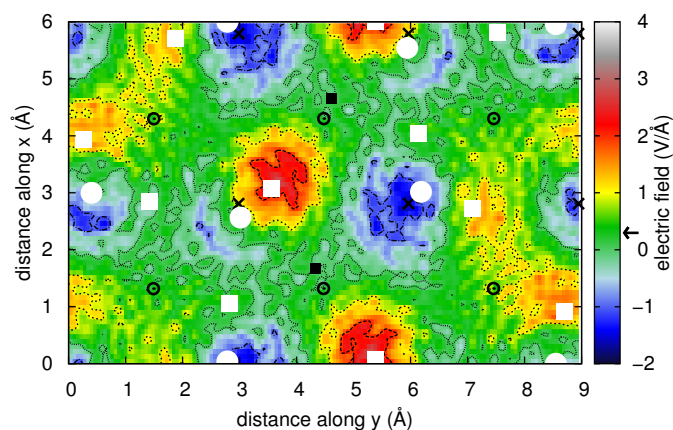


**Fig. 6**  $z$ -component of the electric field in an  $xy$  plane at  $4.0 \text{ \AA}$  from the surface layer of  $\text{MgO}(001)$ . Lines are  $1.0 \text{ V/\AA}$  apart. Underlying atomic positions are labeled with crosses for Mg and circles for O, and squares for H. White circles and squares show the positions of the oxygen and hydrogen atoms in the adsorbed layer. Black squares show the chemisorbed hydrogen atoms. The arrow on the colourbar indicates the average value of the  $z$ -component of the field in this plane.

and statistics were taken from after the simulation had had time to thermalize. The electrostatic potential was dumped every 30 timesteps, for analysis of the electric field throughout the simulation. The electric field profile was obtained as outlined in section 3.1, by averaging the derivative of the potential along  $x$  and  $y$ , and by filtering out the small range oscillations. However, although the  $a/2$  averaging window is appropriate to smooth out oscillations within the  $\text{MgO}$  slab, the water in between the slabs does not exhibit  $a/2$  periodicity along  $z$ . A second filter has been applied in order to smooth out oscillations due to liquid water. This filter was chosen based on the first peak in the oxygen-oxygen pair correlation function using a filter window of  $2.5 \text{ \AA}$ . Other filters were also trialled and it was found that the profile is not very sensitive to the precise size of the window in the liquid, provided the filter window was between  $2.3 \text{ \AA}$ – $2.8 \text{ \AA}$ . Figure 7 shows the electric field profile, density of water, and proton hopping events during 13 ps of simulation at 300 K. The field and density are averages taken over the time of the simulation, and the number of proton hops refers to the number of times an oxygen atom has exchanged one of its two nearest neighbour hydrogens. The figure shows that the electric field at the interface remains intense despite screening by the first layer and subsequent layers of water molecules. When comparing this profile to the 1ML profile in figure 5, there are two main differences: the loss of the double peak and the decrease of field intensity. These differences are both mostly due to the smoothing mentioned above, as without smoothing the  $z$  com-

ponent of the field remains largely unchanged from the single monolayer case. Oscillations of the field in between the slabs are the result of local water dipoles and one would expect that over a long enough simulation or for a large enough box the field in the water far away from the surface would average to zero. The simulation is on small time and length scales which does not give access to the macroscopic values in bulk water; however when the oxygen-oxygen pair correlation function is calculated (see figure 8), we can say that water beyond the first layer is ‘bulk-like’ in that the O-O distances remain very similar to those in the bulk water reference.

The second graph in figure 7 shows oxygen atom and hydrogen atom presence along  $z$ . The oxygen atoms belonging to the  $\text{MgO}$  slab have been omitted for clarity. The first peak of hydrogen presence occurs just above the surface and corresponds to the hydrogen atoms adsorbed directly on the surface. These remain close to their initial positions throughout the simulation and do not re-associate with a water molecule. The second peak shows high oxygen and hydrogen presence, which reflects the stability of the first layer – throughout the simulation, the 6 adsorbed water molecules on each side do not diffuse towards the  $z \approx 0$  region, where there is on average a lower water density. The stability of this first layer is further shown when looking at the oxygen-oxygen pair correlation function in the top part of figure 8. The structure of the monolayer remains largely unchanged when more water molecules are added, with a strong collapse of the second neighbour peak compared to liquid water. This type of structuring on  $\text{MgO}(001)$  has been proposed to resemble a high density ice phase<sup>38</sup>, and could be attributed to a template effect. However, interestingly, similar structural properties have been seen in simulations where there is little or no templating, such as on  $\text{BaF}_2$  in which the first layer exhibits an O-O pair correlation function resembling that of high density liquid water<sup>39</sup>. The high density water layer adsorbed on  $\text{MgO}(001)$  is followed directly by a depleted zone, something that has already been reported in studies of water on other oxide surfaces<sup>10,40</sup> and even on graphene and h-BN<sup>41,42</sup>. In the case of oxides, the initial affinity of the surface for water seems reversed after one layer of coverage – a ‘hydrophilic’ surface can become ‘hydrophobic’ once wet<sup>10</sup>.

### 3.4 Surface-assisted proton transfer

The green histogram in figure 7 was obtained by counting the number of times an oxygen atom had a switch in one of its two nearest neighbour hydrogen atoms, thus counting the number of proton transfer, or ‘proton hopping’ events. In the  $(2 \times 3)$  reconstruction shown in figure 4, proton transfer is susceptible to occur, simply because the high density of the adsorbed layer means that the oxygen atoms are near enough to each other, and also because the layer is partly dissociated which

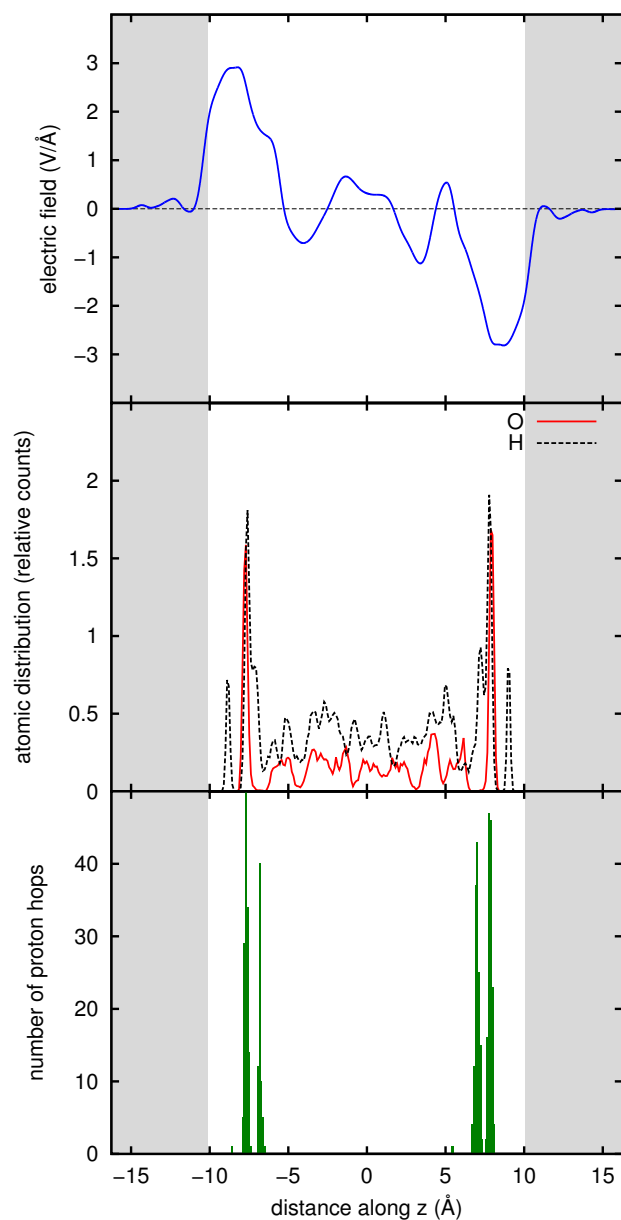


**Fig. 7** The average electric field profile (blue), atomic distribution profiles (red and black) and proton hop counts (green) in the simulation box. Shaded areas correspond to the position of the MgO slabs, to show clearly the position of the interfaces, at  $\pm z_s$  ( $z_s=10.1\text{Å}$ ).

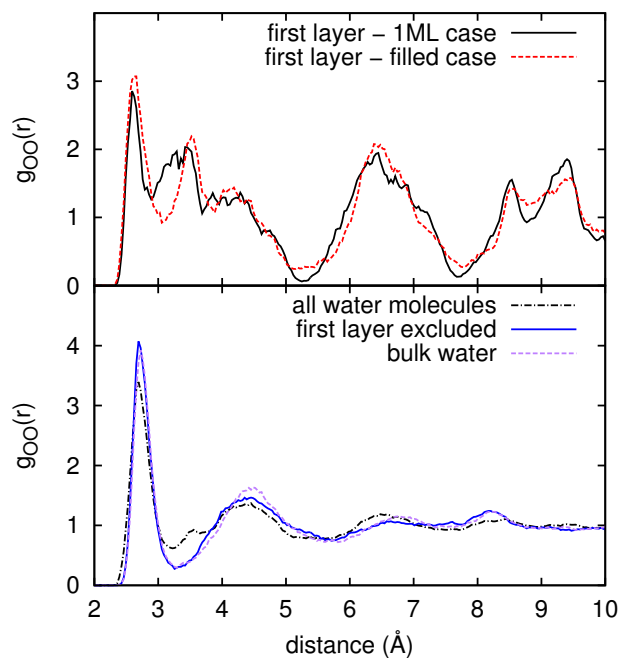


**Fig. 8** O-O pair correlation function in the interfacial water. The top panel compares the O-O distances in the first layer only – the black line for the single adsorbed monolayer simulation, and the red line in the filled case. The second panel compares O-O distances in the filled water simulation (black dashed and blue lines) with O-O distances in a reference simulation of bulk water (purple line).

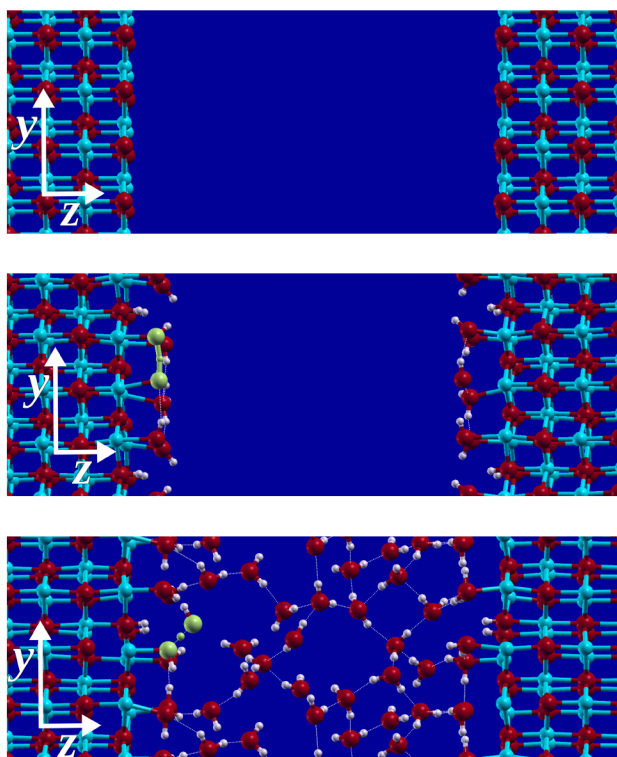


**Fig. 9** Snapshots of the MgO(001), MgO(001)/1ML and MgO(001)/water simulations. In the 1ML and water cases, a proton hopping event is highlighted.

means there are OH groups free to receive the hopping proton from a neighbouring water molecule. Thus it is possible to imagine further metastable configurations from figure 4, and these were observed frequently in our 300K simulation. Such frequent proton transfer at an oxide surface has also been observed in simulations of ZnO<sup>43</sup>. There are two peaks on each side of the histogram. The peak closest to the surface counts the proton transfers within the adsorbed layer, parallel to the surface. The second peak is less intense, and corresponds to hydrogen bonds in the *z* direction. As shown in the third snapshot in figure 9 this corresponds to proton transfer events between the first adsorbed layer and the second layer. It has been recently shown that strong external electric fields promote molecular dissociation and proton hopping in bulk water<sup>44</sup>, ice<sup>45,46</sup>, liquid methanol<sup>47</sup>, as well as a strong chemical reactivity in molecular mixtures<sup>48</sup>. In this case we notice that proton transfer occurs in the first and second layers above the surface corresponding to the zones of highest electric field. Proton transfer in water has also been shown to be correlated to short oxygen-oxygen distance. For instance in the simplest case, the Zundel ion, there is a threshold of oxygen-oxygen distance under which the excess proton prefers to lie in the centre of the two oxygen atoms. In the DFT framework this distance is found to be 2.5 Å although more precise treatments of the problem finds this distance to be closer to 2.4 Å<sup>49</sup>. Classically, proton transfer is expected to occur when the oxygen atoms are closer than this minimum distance, apart from processes of tunnelling, where a quantum treatment of the proton is needed<sup>50</sup>. Figure 10 shows distributions of the oxygen-oxygen distances for hydrogen bonded water molecules, in the first and second layers, and in the other water molecules. With regard to proton transfer, it is important to note that the O-O distances concerned are those which are below the threshold mentioned above. It is clear that there are more very short O-O distances near the surfaces than in the middle of the simulation box. The layers nearest the surfaces have more than 10% of their O-O distances below the DFT proton-hopping threshold, while those in the next slice have between 5% and 10%. Although some bulk water properties seem to be recovered just after the first layer, the heightened density seems to permeate through to the second layer and promote proton transfer. Although proton transfer is more likely when there are more O-O distances well below the threshold, this is not the only driving force for the transfer. Thus the percentage of O-O distances lying below the threshold is not linearly representative of the number of hops. The average shortening time during which an O-O distance stays below 2.5 Å is also found to be correlated with proximity to the surface – with averages of 33, 29, and 21 fs in the first and second layers, and in the bulk, respectively. In this particular study, the proton transfer results in a net transfer of OH<sup>-</sup> ions, as these are initially present on the surface. This type of transfer has been shown to

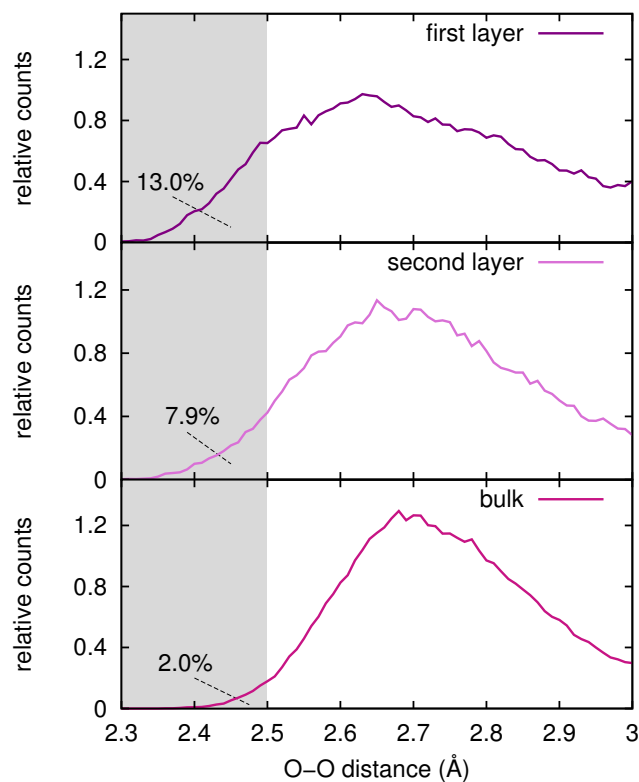


**Fig. 10** Distributions of the Oxygen-Oxygen distances in the water between the slabs, by layer. The first layer refers to the water molecules within  $2\text{\AA}$  of the surface on either side of the slab, while the second layer refers to those between  $2\text{\AA}$  and  $4\text{\AA}$  away from the surface. The distribution referring to the remaining water molecules is labelled as ‘bulk’. An area has been shaded to represent the proton transfer threshold, below which proton transfer may happen. The percentages show how much of each distribution is below this threshold.

depend strongly on the local coordination of the  $\text{OH}^-$ , namely  $\text{OH}^-$  ions which accept three hydrogen bonds are more likely to diffuse than those of a higher coordinance<sup>51</sup>.  $\text{OH}^-$  ions on the  $\text{MgO}(001)$  surface accept two hydrogen bonds from water molecules in the monolayer, and can accept a third from the water molecules above. These are in effect undercoordinated, which probably promotes the transfer of the  $\text{OH}^-$  when it is near the surface. Once the  $\text{OH}^-$  is solvated it is no longer undercoordinated with respect to hydrogen bonding. To summarise, there are several ways in which the surface assists proton transfer: the presence of undercoordinated  $\text{OH}^-$  ions, shorter O-O distances, and a high electric field environment. Possible perspectives include a finer analysis of how these factors are correlated to each other and how they quantitatively affect proton transfer.

## 4 Conclusion

In conclusion, we have presented the first fully atomistic AIMD study of the interface of  $\text{MgO}(001)$  with several layers of liquid water, with particular focus on the so far overlooked surface electric field. Our study yields a few significant conclusions:

Non-polar, defectless surfaces, such as our model  $\text{MgO}(001)$  one, may exhibit high electric fields at distances of up to  $3\text{\AA}$ . When a single monolayer of water molecules is added, the electric field is less intense but still present, and furthermore the zone of high field seems to be broadened to about  $5\text{\AA}$  from the original surface. In a way, this first layer of water serves to spread the high-field interfacial region. Upon adding several layers of water, and after a coarse graining of the field, the  $5\text{\AA}$  window above the surface in which the electric field is high ( $1 - 3\text{ V/\AA}$ ) remains. There is a clear difference between the water molecules belonging to the first layer, which keep close to their initial configuration, and the other water molecules which are free to diffuse. The atomic density profiles show a depleted zone just above the adsorbed layer, and the O-O pair correlation function is similar to that of bulk water once the first adsorbed layer is not taken into account.

Proton transfer occurs at the  $\text{MgO}(001)$ /water interface, and this is observed at significant rates on AIMD-accessible timescales. Our results show that proton transfer occurs in the zone close to the surface where the electric field is strongest. This can be partly explained by a higher proportion of small O-O distances in those zones.

In perspective, our study suggests that local electric fields at the surface of dry and wet oxides and minerals are sufficiently intense, even in clean, flat, and apolar surfaces as  $\text{MgO}(001)$ , to promote molecular dissociations, and thus to modify the free energy landscape of surface chemical reactions, with important consequences in geochemistry.

## 5 Acknowledgments

This work was granted access to the HPC resources of IDRIS under the allocation 2015091387 made by GENCI. We acknowledge the Île-de-France Region for funding via the DIM OxyMORE.

## References

- 1 G. E. Ewing, *Chem. Rev.*, 2006, **106**, 1511–1526.
- 2 A. Marshall, B. Børresen, G. Hagen, M. Tsytkin and R. Tunold, *Mater. Chem. Phys.*, 2005, **94**, 226 – 232.
- 3 J. Rossmeißl, Z.-W. Qu, H. Zhu, G.-J. Kroes and J. Nørskov, *J. Elec. Chem.*, 2007, **607**, 83 – 89.

- 4 A. N. Cormack and A. Tilocca, *Phil. Trans. R. Soc. A*, 2012, **370**, 1271–1280.
- 5 A. Motta, M.-P. Gaigeot and D. Costa, *J. Phys. Chem. C*, 2012, **116**, 23418–23427.
- 6 A. Tilocca and A. N. Cormack, *Appl. Mater. Interf.*, 2009, **1**, 1324–1333.
- 7 F. Musso, P. Mignon, P. Ugliengo and M. Sodupe, *Phys. Chem. Chem. Phys.*, 2012, **14**, 10507.
- 8 H. Sakuma, T. Tsuchiya, K. Kawamura and K. Otsuki, *Mol. Simul.*, 2004, **30**, 861.
- 9 G. Cicero, J. C. Grossman, A. Catellani and G. Galli, *J. Am. Chem. Soc.*, 2005, **127**, 6830–6835.
- 10 B. Rotenberg, A. J. Patel and D. Chandler, *J. Am. Chem. Soc.*, 2011, **133**, 20521–20527.
- 11 P. Geysersmans, F. Finocchi, J. Goniakowski, R. Hacquart and J. Jupille, *Phys. Chem. Chem. Phys.*, 2009, **11**, 2228–2233.
- 12 G. Jordanand, S. R. Higgins and C. M. Eggleston, *Am. Mineral.*, 1999, **84**, 144.
- 13 D. Costa, C. Chizallet, B. Ealet, J. Goniakowski and F. Finocchi, *J. Chem. Phys.*, 2006, **125**, 054702.
- 14 R. S. Alvim, I. B. Jr, D. G. Costa and A. A. Leitao, *J. Phys. Chem. C*, 2011, **116**, 738.
- 15 P. Liu, T. Kendelewicz, G. E. Gordon and G. A. Parks, *Surf. Sci.*, 1998, **413**, 287.
- 16 J. T. Newberg, D. E. Starr, S. Yamamoto, S. Kaya, T. Kendelewicz, E. R. Mysak, S. Porsgaard, M. B. Salmeron, G. E. Brown, A. Nilsson and H. Bluhm, *J. Phys. Chem. C*, 2011, **115**, 12864–12872.
- 17 R. Włodarczyk, M. Sierka, K. Kwapien, J. Sauer, E. Carrasco, A. Aumer, J. F. Gomes, M. Sterrer and H.-J. Freund, *J. Phys. Chem. C*, 2011, **115**, 6764–6774.
- 18 L. Giordano, J. Goniakowski and J. Suzanne, *Phys. Rev. Lett.*, 1998, **81**, 1271–1273.
- 19 C. Toubin, S. Picaud and C. Girardet, *Chem. Phys.*, 1999, **244**, 227–249.
- 20 H. S. Craft, R. Collazo, M. D. Losego, Z. Sitar and J.-P. Maria, *J. Vac. Sci. Technol. A*, 2008, **26**, 1507–1510.
- 21 M. Foster, M. D’Agostino and D. Passno, *Surf. Sci.*, 2005, **590**, 31.
- 22 N. H. de Leeuw and S. C. Parker, *PRB*, 1998, **58**, 13901.
- 23 V. Shapovalov, T. N. Truong, A. Kovalenko and F. Hirata, *Chem. Phys. Lett.*, 2000, **320**, 186–193.
- 24 D. Spagnoli, J. P. Allen and S. C. Parker, *Langmuir*, 2011, **27**, 1821–1829.
- 25 S. A. Deshmukh and S. K. R. S. Sankaranarayanan, *Phys. Chem. Chem. Phys.*, 2012, **14**, 15593–15605.
- 26 F. Tielens and C. Minot, *Surf. Sci.*, 2006, **600**, 357.
- 27 M. Ončák, R. Włodarczyk and J. Sauer, *The Journal of Physical Chemistry Letters*, 2015, **6**, 2310–2314.
- 28 M. Nonnenmacher, M. P. O’Boyle and H. K. Wickramasinghe, *Applied Physics Letters*, 1991, **58**, year.
- 29 Y. Xu, J. Li, Y. Zhang and W. Chen, *Surface Science*, 2003, **525**, 13–23.
- 30 M. Otani and O. Sugino, *Phys. Rev. B*, 2006, **73**, 115407.
- 31 L. Vlcek, Z. Zhang, M. L. Machesky, P. Fenter, J. Rosenqvist, D. J. Wesolowski, L. M. Anovitz, M. Predota and P. T. Cummings, *Langmuir*, 2007, **23**, 4925–4937.
- 32 A. D’Ercole, A. M. Ferrari and C. Pisani, *J. Chem. Phys.*, 2001, **115**, 509–518.
- 33 S. M. Kathmann, I.-F. W. Kuo, C. J. Mundy and G. K. Schenter, *J. Phys. Chem. B*, 2011, **115**, 4369–4377.
- 34 P. Giannozzi, S. Baroni, N. Bonini, M. Calandra, R. Car, C. Cavazzoni, D. Ceresoli, G. L. Chiarotti, M. Cococcioni, I. Dabo, A. Dal Corso, S. de Gironcoli, S. Fabris, G. Fratesi, R. Gebauer, U. Gerstmann, C. Gougoussis, A. Kokalj, M. Lazzeri, L. Martin-Samos, N. Marzari, F. Mauri, R. Mazzarello, S. Paolini, A. Pasquarello, L. Paulatto, C. Sbraccia, S. Scandolo, G. Sclauzero, A. P. Seitsonen, A. Smogunov, P. Umari and R. M. Wentzcovitch, *J. Phys. Condens. Matter*, 2009, **21**, 395502.
- 35 S. Grimme, *J. Comput. Chem.*, 2006, **27**, 1787–1799.
- 36 M. Peressi, N. Binggeli and A. Baldereschi, *J. Phys. D Appl. Phys.*, 1998, **31**, 1273.
- 37 J. Y. Lim, J. S. Oh, B. D. Ko, J. Won Cho, S. O. Kang, G. Cho, H. S. Uhm and E. H. Choi, *J. Appl. Phys.*, 2003, **94**, 764–769.
- 38 J. Coulomb, B. Demirdjian, D. Ferry and M. Trabelsi, *Adsorption*, 2013, **19**, 861–867.
- 39 S. Kaya, D. Schlesinger, S. Yamamoto, J. T. Newberg, H. Bluhm, H. Ogasawara, T. Kendelewicz, G. Brown, L. G. M. Pettersson and A. Nilsson, *Sci. Rep.*, 2015, **3**, 1074.
- 40 S. J. Cox, Z. Raza, S. M. Kathmann, B. Slater and A. Michaelides, *Faraday Discuss.*, 2013, **167**, 389–403.
- 41 G. Cicero, J. C. Grossman, E. Schwegler, F. Gygi and G. Galli, *J. Am. Chem. Soc.*, 2008, **130**, 1871–1878.
- 42 G. Tocci, L. Joly and A. Michaelides, *Nano Letters*, 2014, **14**, 6872–6877.
- 43 G. Tocci and A. Michaelides, *The Journal of Physical Chemistry Letters*, 2014, **5**, 474–480.
- 44 A. M. Saitta, F. Saija and P. V. Giaquinta, *Phys. Rev. Lett.*, 2012, **108**, 207801.
- 45 G. Cassone, P. V. Giaquinta, F. Saija and A. M. Saitta, *J. Phys. Chem.*, 2014, **118**, 12717–12724.
- 46 G. Cassone, P. V. Giaquinta, F. Saija and A. M. Saitta, *J. Phys. Chem. B*, 2014, **118**, 4419–4424.
- 47 G. Cassone, P. V. Giaquinta, F. Saija and A. M. Saitta, *J. Chem. Phys.*, 2015, **142**, 054502.
- 48 A. M. Saitta and F. Saija, *Proc. Natl. Acad. Sci.*, 2014, 13768–13773.
- 49 M. Dagrada, M. Casula, A. M. Saitta, S. Sorella and F. Mauri, *J. Chem. Theory Comput.*, 2014, **10**, 1980–1993.
- 50 Y. Bronstein, P. Depondt, F. Finocchi and A. M. Saitta, *Phys. Rev. B*, 2014, **89**, 214101.
- 51 Z. Ma and M. E. Tuckerman, *Chemical Physics Letters*, 2011, **511**, 177–182.